

# Bioinspired Phosphatase-like Mimic Built from the Self-Assembly of De Novo Designed Helical Short Peptides

Yutong Wang, Lijun Yang, Mengfan Wang,\* Jiaxing Zhang, Wei Qi,\* Rongxin Su, and Zhimin He



Cite This: *ACS Catal.* 2021, 11, 5839–5849



Read Online

ACCESS |



Metrics & More



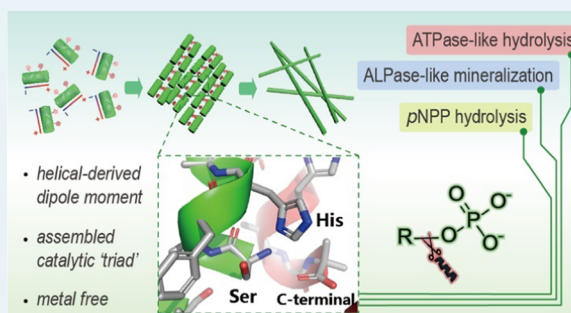
Article Recommendations



Supporting Information

**ABSTRACT:** Enzymes play vital roles in catalyzing biochemical reactions with high activity and selectivity, which is largely attributed to the delicately organized structure and groups at catalytic domains. Reconstruction of the enzymatic catalytic domains in artificial systems, to produce enzyme-like mimic, has become an attractive but challenging subject. Herein, inspired by the helical structure in the catalytic center of natural phosphatases, we created a phosphatase-like mimic through the self-assembly of de novo designed helical heptapeptides. The helical heptapeptides were elaborately decorated with well-studied catalytic groups and exhibited obvious phosphatase-like catalytic activity upon hierarchically self-assembling. In comparison with  $\beta$ -sheet-organized peptide assemblies, we emphasized the significance of helical structure in the hydrolysis of phosphoester bonds (over 1000 times higher in catalytic efficiency). The structure–activity relationship reveals that the phosphatase-like function attributed to the specific helical dipole moment for the binding of substrates as well as the supramolecular assembly for the formation of catalytic center. Moreover, we verified the feasibility of these helical species as a potential substitute for adenosine triphosphatase (ATPase) and alkaline phosphatase (ALPase) in some specific biological processes. This work not only presents an approach for the construction of artificial enzymes with simple peptide modules but also provides a model for primitive enzymes formed from helical short peptides that relied on self-assembly to achieve a folded structure.

**KEYWORDS:** enzymatic mimics, helical peptide, phosphoester bond hydrolysis, de novo design, self-assembly



## 1. INTRODUCTION

As biocatalysts, enzymes have evolved into special substances that play amazing roles in biological metabolism, nutrition, and energy conversion, and they have shown outstanding efficiency, specificity, and stereoselectivity in industrial fields. As substitutes for natural enzymes, the construction of artificial mimics with enzyme-like functions has become an exciting field over the past decades, including synthetic peptides,<sup>1–3</sup> nucleic acids,<sup>4–6</sup> metal–organic complexes,<sup>7–9</sup> and metal oxides.<sup>10–12</sup> Except for some ribonucleic acids, most enzymes are proteins with well-organized three-dimensional structures. Currently, based on the delicate structure of natural enzymes, many supramolecular approaches have been developed for the reconstruction of the enzymatic active sites in artificial systems.<sup>13,14</sup> Unfortunately, this approach is sometimes arduous due to the insufficient understanding of the structure–function relationship of enzymes and the chemical differences between artificial materials and natural proteins.

More anticipated but even more challenging is the design of a protein module with a predictable structure and catalytic function.<sup>15,16</sup> One of the philosophies from the engineering field is the design and construction of standard parts or components, which can perform specific tasks in different contexts. At the protein level, this “plug-and-play” manner is

quite common in natural enzymes: domains with similar peptide sequences, catalytic groups, or structures have the same role in different systems.<sup>17</sup> Fortunately, some principles and methodologies have been developed to design peptides with definite conformation or function.<sup>18–21</sup> This inspired us to create a simple peptide module, rather than an entire protein or artificial material to replicate the structure of catalytic domains and mimic the functions of natural enzymes.

Recently, the achievements of catalytic amyloids from  $\beta$ -sheet peptide self-assembly show the way from concept to practice. Through the rational design of assembling peptide sequences, the catalytic domains of natural enzymes can be replicated by simple peptide modules. For example, Korendovych et al. designed a series of  $\beta$ -sheet-forming heptapeptides and obtained a Zn(II)-coordinated structure through the self-assembly of these peptides. The structure replicated the catalytic center of natural carbonic anhydrase,

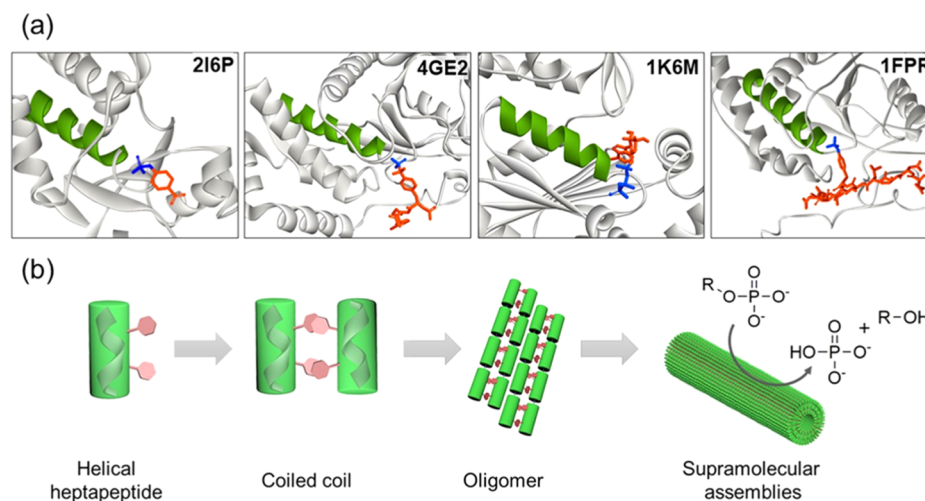
**Received:** January 11, 2021

**Revised:** April 9, 2021

**Published:** April 28, 2021



Scheme 1. (a) Catalytic Centers of Some Metal-Free Phosphoester Hydrolysis Enzymes (data from www.rcsb.org, PDB ID: 2I6P, 4GE2, 1K6M, and 1FPR);<sup>a</sup> (b) Hierarchical Self-Assembly of Helical Peptides into Supramolecular Assemblies with Phosphatase-like Activity



<sup>a</sup>The N-terminal of the  $\alpha$ -helix (green) points to the phosphate group (highlighted in blue) of the substrate (orange molecule).

showing catalytic ability toward the substrates of carbonic anhydrase.<sup>22</sup> Numata et al. constructed an enzyme-like catalyst by introducing the classical serine-protease catalytic triad into peptides that can self-assemble into amyloid-like fibrils. They found that the formation of the  $\beta$ -sheet backbone is crucial in organizing the protease-like active site.<sup>23</sup>

Although many enzyme mimics have been realized based on  $\beta$ -sheet peptides self-assembly, very little attention has been paid to  $\alpha$ -helix motifs. Actually, helical structure dominates almost 30% of globular protein segments on average and takes charge of many irreplaceable functions, such as DNA-binding sites and proton channels.<sup>24,25</sup> This prompted us to explore the roles of helical structures in some natural enzymes and attempt to design a similar helical module to execute supramolecular assemblies with enzyme-like functions. It is well-known that the spontaneous hydrolysis of phosphoester bonds is extremely slow, with a cleavage half-life of  $\sim 10^7$  years.<sup>26</sup> In living organisms, the highly effective hydrolysis of phosphoester bonds is related to various metal-containing or metal-free phosphatase families,<sup>27</sup> which play vital roles in energy production, signal transduction, bone formation, and gene maintenance. The protein crystal structure revealed that  $\alpha$ -helical motifs are ubiquitous in the catalytic domain of phosphatase families,<sup>28</sup> especially for those metal-free phosphatases in which metal cofactors are absent in the active site. The instinctive dipole of the helical structure promotes the binding of negatively charged phosphate substrates to the N-terminal of the helix and the consequent enhancing of the attack toward phosphoester bonds (Scheme 1a).<sup>29</sup> Inspired by this, we wondered whether a self-assembled helical short peptide could possess the phosphatase-mimicking active site and exhibit phosphatase-like catalytic function.

To achieve this goal, in this study, bioinspired de novo design was performed to obtain a coiled-coil-forming helical heptapeptide. As a unique association of helical peptides that assemble into a superhelix structure, coiled coil often serves as the basic module in many biological recognition processes.<sup>30</sup> By installing catalytic residues into the helical heptapeptides, we created a metal-free phosphatase mimic through the hierarchical self-assembly of helical heptapeptides into supra-

molecular assemblies (Scheme 1b). A hydrolytic reaction using *p*-Nitrophenyl phosphate (*p*NPP) as a model substrate confirmed the unique phosphatase-like catalytic activity of helical assemblies. By comparing with  $\beta$ -sheet-organized peptide assemblies, we highlighted the significance of helical structure in phosphate ester hydrolysis. Based on the X-ray diffraction analysis and computer simulation, the structure–activity relationship was investigated to demonstrate the function of the helical dipole moment and supramolecular assembly in phosphatase-like catalysis. Moreover, we also verified the feasibility of this helical species as a potential substitute for adenosine triphosphatase (ATPase) and alkaline phosphatase (ALPase) in specific biological processes. This work presents a bioinspired phosphatase-like mimic via the self-assembly of short helical peptides in the absence of any metal cofactor and also shows the possibility of the construction of artificial enzymes based on the self-assembly of well-understood and completely de novo designed short peptides.

## 2. RESULTS AND DISCUSSION

**2.1. Peptide Sequence Design.** To highlight the significance of the helical structure for the phosphatase-mimicking structure and function, a helical sequence that is as simple as possible is required. Coiled coil is a structural motif in proteins in which helices are coiled together like the strands of a rope. The peptide sequence of a coiled coil usually followed the heptad repeat pattern of (*hpphpp*)<sub>*n*</sub>, or named under *abcdefg* rule.<sup>31,32</sup> In the repeat sequence, the *a* and *d* positions are usually occupied by hydrophobic (*h*) residues, and the *b*, *c*, *e*, *f*, and *g* positions are occupied by polar (*p*) residues. In the folded state, the hydrophobic residues present a periodic hydrophobic interface (*a–d* faces) and act as an oligomerization domain during the association of two or more such helical units. Driven by the *a–d* faces, the average 3.5-residue spacing of hydrophobic side chains in heptad repeats is very close to the typical 3.6-residue repeat of  $\alpha$ -helix, resulting in the formation of amphiphilic helices that are wrapped around each other in a right-handed style (Figure 1). In a recent study, Gazit et al. reported a heptapeptide (SHR-FF)

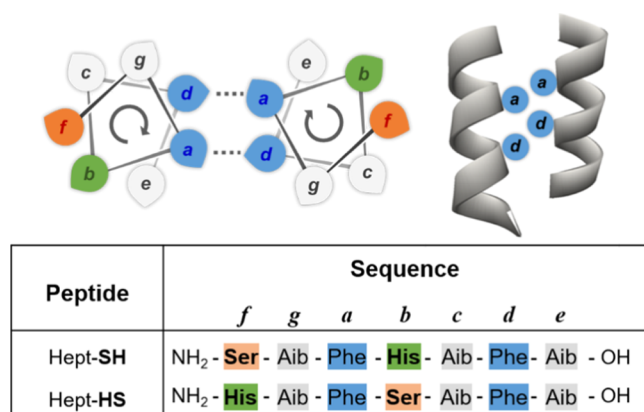


Figure 1. Design of Catalytic Helical Heptapeptides.

which is able to form coiled-coil assemblies.<sup>33</sup> The peptide sequence followed the typical *abcdefg* rule. In this study, a similar helical heptapeptide was designed by integrating hydrophobic phenylalanine (Phe, F) into the *a* and *d* positions to form a “phenylalanine zipper”. To overcome the thermodynamic barrier in helical folding, a noncoded amino acid  $\alpha$ -aminoisobutyric acid (Aib) was incorporated at the *c*, *e*, and *g* positions. The additional  $\alpha$ -methyl group in Aib limits the ranges of allowed  $\varphi$ ,  $\psi$  torsion angles compared with alanine and imposes restrictions over the energetically accessible conformational space, which thus stabilizes the helical configuration.<sup>34</sup> To guarantee the basic helical structure, the heptapeptide sequence was minimally mutated with catalytic residues for the purpose of enzyme-like catalysis.

Based on the delicate electron-transfer system of the catalytic triad in general hydrolases,<sup>35</sup> the sequence involved the decoration of serine (Ser, S) and histidine (His, H) residues within the backbone as well as the carboxyl at the C-terminal. Serine and histidine were assigned to the positions of *b* and *f*, which hence has a minimal effect on helical folding. Taking the orientation into consideration, two variants were assigned by exchanging the positions of Ser and His at the *b* and *f* positions, leading to the species of Hept-SH and Hept-HS (Figure 1). Their influences on the structure and catalysis ability of helical assemblies were also investigated in this study.

## 2.2. Peptide Assembly and Structural Investigation.

The designed peptides were obtained by standard solid-phase synthesis, purified by reversed-phase high-performance liquid chromatography (HPLC), and confirmed by electrospray ionization (ESI) mass spectrometry (Figures S1 and S2). In a typical procedure, the self-assembly of heptapeptides was launched by dissolving a certain amount of heptapeptides into dimethyl sulfoxide (DMSO), followed by mixing the peptide stock with a neutral buffer. The fibrillar nanostructure in the transmission electron microscopy (TEM) images implied the well-organized self-assembly of Hept-SH and Hept-HS (Figure 2a,b). Circular dichroism (CD) was performed to investigate the secondary structure of peptide molecules in the assemblies (Figure 2c). The spectra displayed a double-negative Cotton effect around 204 and 214 nm along with a positive peak at 196 nm, which is the characteristic pattern of the helical conformation built by short peptides.<sup>36–38</sup> Compared with the spectrum of typical  $\alpha$ -helix in proteins, the shorter length of the helix results in a slight blue-shift of the characteristic peaks by 3–7 nm and a lower intensity of the signals.<sup>39,40</sup> This result

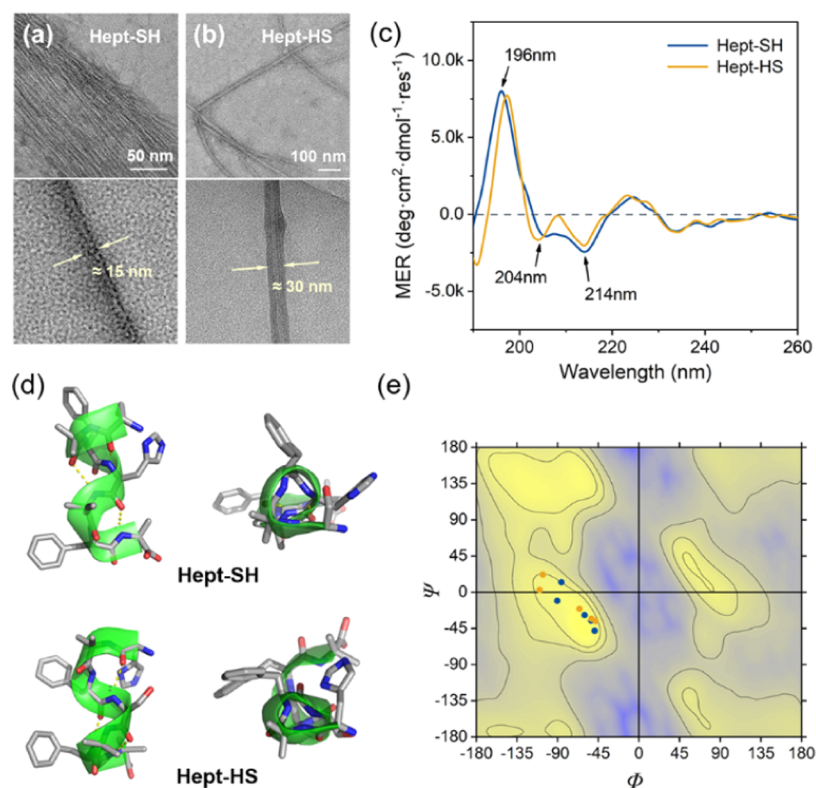
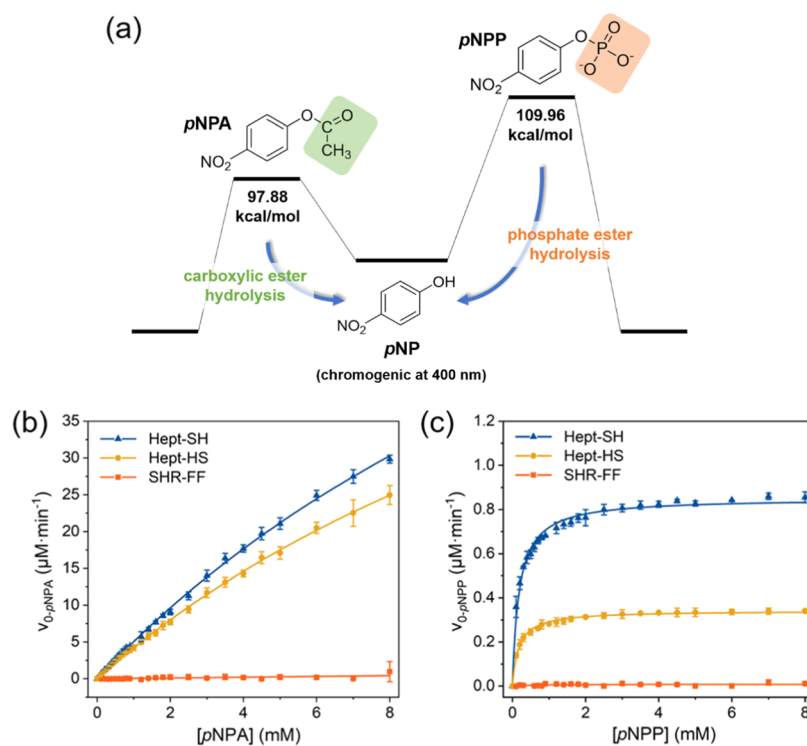


Figure 2. TEM images of (a) Hept-SH and (b) Hept-HS assemblies. (c) CD spectra of the heptapeptides. (d) Different configurations of Hept-SH and Hept-HS helices. (e) Torsion angles of the residues in Hept-SH (blue dots) and Hept-HS (yellow dots) superimposed over the ideal Ramachandran plot.



**Figure 3.** (a) Bond cleavage energies along with the hydrolysis reactions of *p*NPA and *p*NPP. Initial rate ( $V_0$ ) of the hydrolysis reaction as a function of (b) *p*NPA or (c) *p*NPP concentration catalyzed by 0.08 mM helical assemblies. The data in (b) and (c) are smoothed fitting with the Michaelis–Menten equation.

was also supported by attenuated total reflectance-infrared Fourier transform infrared (ATR-FTIR) and Raman spectra (Figures S7 and S8).<sup>41–43</sup> The secondary structure assignment based on amide I and amide III bands showed that helical structures dominated the backbones of both heptapeptides.

NMR spectroscopy was employed to reveal the structures of folded peptides in a solution.<sup>44,45</sup> The strong and clear nonsequential NOE constraints indicated the typical  $H_i-H_{i+3}$  correlations within the heptapeptide molecules (Figures S9 and S10), which followed the character of  $3_{10}$ -helix.<sup>46</sup> X-ray crystallography revealed the precise structures of the peptide molecules. As shown in Figure 2d, the peptide backbone of Hept-SH and Hept-HS displayed the typical helical configuration. Ramachandran plot indicated that the torsion angles of all residues coincided well with the right-handed helical configuration (Figure 2e and Tables S1 and S2).<sup>47</sup> Unlike SHR-FF, where water molecules bridge N–H and O=C groups via hydrogen bonds,<sup>33</sup> Hept-SH and Hept-HS formed three intramolecular hydrogen bonds directly between N–H and O=C groups located at the *i* and *i*+3 positions, which promotes the stable folding of the helical structure (Figure S11). When viewed from the N-terminal, the backbone of heptapeptides exhibited a typical  $3_{10}$ -helix configuration. Due to the steric hindrance of imidazole in histidine, Hept-SH formed a hydrogen bond between the *g* and *c* residues. For Hept-HS, the histidine at the *b* position was replaced by serine, leading to the formation of a hydrogen bond between *a* and *d*. We speculated that this variation enhanced the hydrophobic or  $\pi$ – $\pi$  interactions between the phenylalanine side chains at the *a* and *d* positions, which constrained Hept-HS to adopt a more rigid helical folding than Hept-SH. Both heptapeptide helices showed favorable thermal stability even though the temperature rose to 90 °C (Figure S12).

**2.3. Phosphatase-like Catalytic Ability.** After demonstrating the helical structure of the designed heptapeptides, we further investigated the phosphatase-like catalytic ability of the heptapeptide assemblies. For comparison, some previously reported  $\beta$ -sheet-organized peptide assemblies were also studied to investigate the different effects of the helical/ $\beta$ -sheet structure on the hydrolysis of the phosphoester bond. It is worth noting that although numerous  $\beta$ -sheet-organized peptide assemblies claimed their hydrolase activity based on the general hydrolytic substrate (*p*-nitrophenyl acetate, *p*NPA), there is little evidence showing their catalytic ability toward phosphoester substrates. Relative bond energy analysis indicated that the cleavage of the phosphate ester bond in *p*NPP requires more energy (109.96 kcal/mol) than destroying the carboxylic ester bond in *p*NPA (97.88 kcal/mol) (Figure 3a). Thus, with respect to thermodynamics, the hydrolysis of the phosphoester substrate is much more difficult than the general substrate. Also, in organisms, the hydrolysis of these two bonds adopts different pathways and enzyme families (carboxylesterases versus phosphatases).<sup>48,49</sup>

Herein, the catalytic ability of helical assemblies toward both the general hydrolytic substrate (*p*NPA) and the phosphate ester substrate (*p*NPP) were evaluated. For the general hydrolytic substrate *p*NPA, the initial hydrolysis rates  $V_0$ -*p*NPA as a function of various *p*NPA concentrations are shown in Figure 3b. The reactions followed the typical Michaelis–Menten model, which confirmed their enzyme-like catalytic behavior. The catalytic rate constant of an enzyme ( $k_{\text{cat}}$ ) is the maximal number of substrate molecules converted to product per active site per unit time,<sup>50</sup> which often reflects the speed for the forward reaction of an enzyme–substrate complex. Herein,  $k_{\text{cat}}$  was obtained based on the linear Lineweaver–Burk plots (Table 1 and Figure S13), indicating that Hept-SH

Table 1. Kinetic Analysis for the Enzyme-like Hydrolysis of *p*NPA and *p*NPP<sup>a</sup>

species	structure	<i>p</i> NPA				<i>p</i> NPP				ref
		$V_{\max}$ ( $\times 10^{-8}$ M·s <sup>-1</sup> )	$k_{\text{cat}}$ ( $\times 10^{-5}$ s <sup>-1</sup> )	$K_m$ ( $\times 10^{-3}$ M)	$k_{\text{cat}}/K_m$ (M <sup>-1</sup> ·s <sup>-1</sup> )	$V_{\max}$ ( $\times 10^{-8}$ M·s <sup>-1</sup> )	$k_{\text{cat}}$ ( $\times 10^{-5}$ s <sup>-1</sup> )	$K_m$ ( $\times 10^{-3}$ M)	$k_{\text{cat}}/K_m$ (M <sup>-1</sup> ·s <sup>-1</sup> )	
Hept-SH	helix	191.79 ± 11.54	2397.39 ± 23.08	22.34 ± 0.26	1.07 ± 0.00	1.47 ± 0.00	18.33 ± 0.00	0.26 ± 0.00	0.70 ± 0.01	this work
Hept-HS	helix	151.10 ± 11.54	1888.79 ± 23.08	20.93 ± 0.29	0.90 ± 0.00	0.59 ± 0.00	7.38 ± 0.00	0.26 ± 0.01	0.28 ± 0.01	this work
SHR-FF	helix	inactive				inactive				33
SA-H	$\beta$ -sheet	ND	200.00	20.03	0.10	inactive				51
CoA-HSD	$\beta$ -sheet	ND	300.00	16.29	0.18	inactive				51
Azo-GFGH	$\beta$ -sheet	ND	366.67	15.56	0.23	inactive				52
F-Zn(II)	amyloid-like	48.5	ND	0.169	76.54	inactive				53
Lauryl-VVAGH-Am	$\beta$ -sheet	ND				ND	1.83	ND	0.00069	54

<sup>a</sup>Kinetic parameters are directly cited from references or calculated from the original data. ND: not determined or not demonstrated in the references.

nanofibers ( $k_{\text{cat}} = 2397.39 \pm 23.08 \times 10^{-5} \text{ s}^{-1}$ ) are more active than Hept-HS assemblies ( $k_{\text{cat}} = 1888.79 \pm 23.08 \times 10^{-5} \text{ s}^{-1}$ ). The hydrolytic ability of helical assemblies on *p*NPA comes from the function of catalytic triad groups involved in the peptide sequence. As a control, SHR-FF, which has been reported to form suprahelical nanofibers in the study by Gazit, displayed scarcely any catalytic activity, due to the lack of catalytic residues.

For the phosphatase-like activity assay, we monitored the product versus time plots for the hydrolysis of *p*NPP (Figure S14). The result demonstrated that the addition of the Hept-SH or Hept-HS assemblies significantly accelerated the hydrolysis of *p*NPP. After 24 h, the *p*NPP yielded the maximum value and the turnover number (TON) reached 253 under the catalysis of Hept-SH nanofibers. As the mutation of Hept-SH, the helical assemblies are almost inactive toward *p*NPP once the catalytic serine or histidine residue in Hept-SH sequence was substituted by neutral residues, such as alanine (Figure S15).

The hydrolysis of *p*NPP by Hept-SH or Hept-HS nanofibers is also consistent with the enzymatic reaction kinetics (Figure 3c), and  $k_{\text{cat}}$  of Hept-SH nanofibers ( $18.33 \pm 0.00 \times 10^{-5} \text{ s}^{-1}$ ) is still higher than that of Hept-HS nanofibers ( $7.38 \pm 0.00 \times 10^{-5} \text{ s}^{-1}$ ). Normally, the spontaneous hydrolysis of *p*NPP is extremely slow ( $k_{\text{uncat}} = 2.7 \times 10^{-9} \text{ s}^{-1}$ ).<sup>55</sup> Here, the helical assemblies showed a  $10^4$ -fold acceleration than the uncatalyzed reaction (Table S3), confirming the obvious phosphatase-mimicking function of Hept-SH and Hept-HS nanofibers. We also noticed that for both helical assemblies, the  $k_{\text{cat}}$  values for the *p*NPP hydrolysis are much lower than those for the *p*NPA hydrolysis (Table 1). This result agrees with Arrhenius' theory ( $\ln k = \ln A - E_a/RT$ ), where the reaction rate is inversely proportional to the energy barrier.<sup>56</sup> In addition, the  $K_m$  values for the hydrolysis of *p*NPP are much lower than those for the hydrolysis of *p*NPA, which implied the superior affinity of helical assemblies toward *p*NPP compared with *p*NPA. Besides SHR-FF, we also detected the catalytic ability of Hept-AH and Hept-SA assemblies in the hydrolysis of *p*NPP.

The comparison of catalytic performances of helical assemblies with those of  $\beta$ -sheet and amyloid-like organizations is more instructive. Catalytic efficiency ( $k_{\text{cat}}/K_m$ ) is a comprehensive parameter to evaluate the catalysis ability of different enzymes toward a certain substrate. Herein, we investigated the catalytic ability of SA-H, CoA-HSD, and Azo-GFGH assemblies toward *p*NPP. These  $\beta$ -sheet peptide assemblies have been proven to be efficient hydrolase mimics in our previous reports ( $k_{\text{cat}}/K_m = 0.1\text{--}0.23 \text{ M}^{-1} \text{ s}^{-1}$ ) according to the activity assay utilizing *p*NPA<sup>51,52</sup> but completely inactive toward *p*NPP (Figure S16). Similar phenomenon occurred to the amyloid-like hydrolase mimic F-Zn(II), which shows hyperactivity toward *p*NPA ( $k_{\text{cat}}/K_m = 76.54 \text{ M}^{-1} \text{ s}^{-1}$ ) but still inactive toward *p*NPP.<sup>53</sup> The significant reactivity of the helical species toward *p*NPP is also recognized when compared with the previously reported phosphatase mimic assembled from the  $\beta$ -sheet-organized Lauryl-VVAGH-Am:<sup>54</sup> the  $k_{\text{cat}}/K_m$  of helical assemblies for the hydrolysis of *p*NPP are  $\sim 1000$  times higher than that of Lauryl-VVAGH-Am assemblies ( $k_{\text{cat}}/K_m = 0.00069 \text{ M}^{-1} \text{ s}^{-1}$ ). Therefore, we validated the phosphatase-like catalytic ability of the helical assemblies and realized the superiority of the helical structure over  $\beta$ -sheet in the hydrolysis of the phosphoester bond.

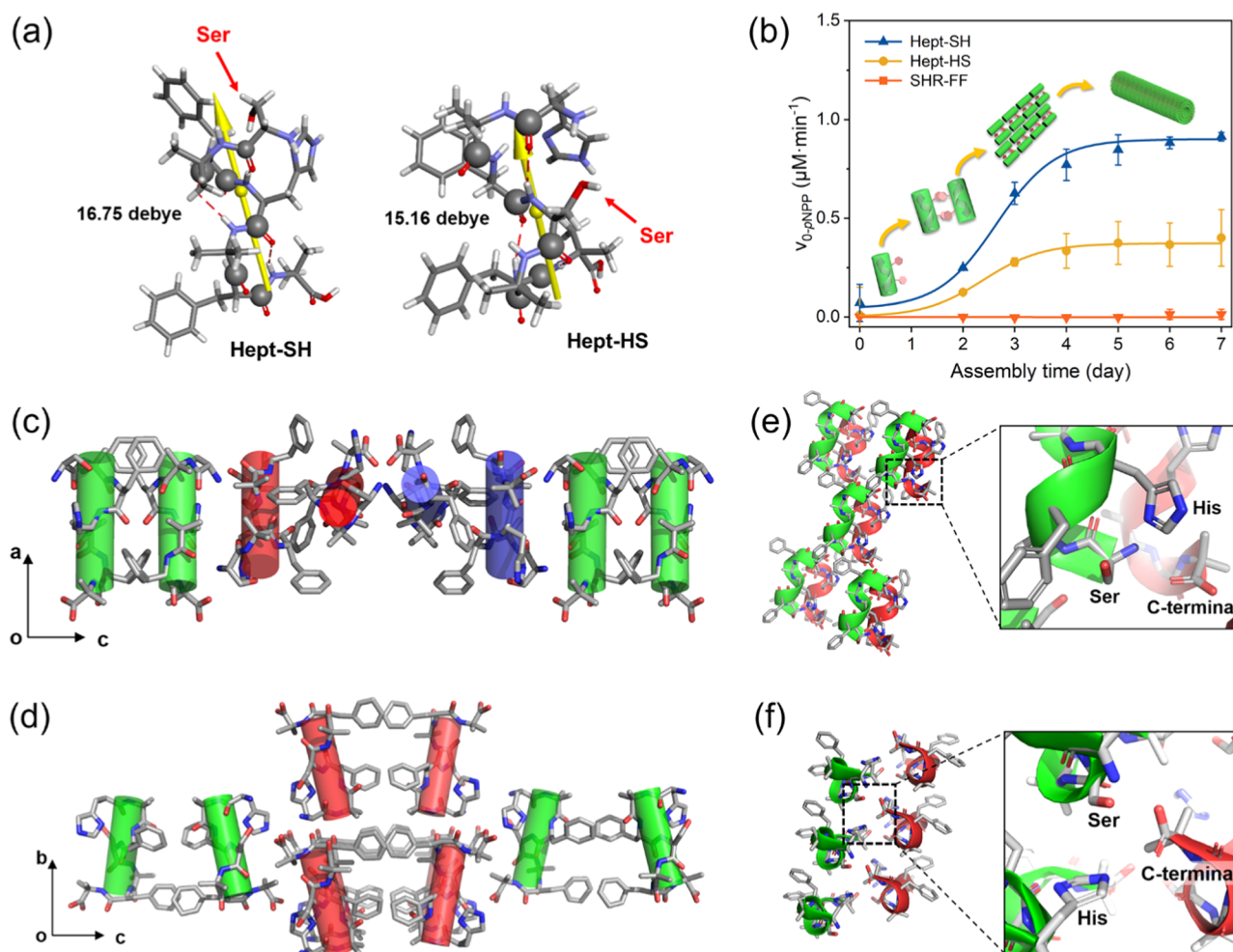


**Figure 4.** (a) Overall effect of the dipole moment (yellow arrow) in Hept-SH and Hept-HS helices obtained by the DFT calculation. The black balls represent the  $\alpha$ -carbon atoms in the peptide backbone. (b) Effect of the assembly time on the hydrolysis rate of pNPP catalyzed by helical assemblies. Higher ordered organization patterns of (c) Hept-SH helices and (d) Hept-HS helices. The catalytic groups in (e) Hept-SH and (f) Hept-HS assemblies. Dimers are differentiated by colors.

Admittedly, the phosphoester bond hydrolysis ability of the helical assemblies are several orders of magnitude lower than that of natural enzymes (e.g., the  $k_{\text{cat}}$  of tyrosine phosphatase is  $8.24 \text{ s}^{-1}$  toward pNPP).<sup>57</sup> However, it is still an exciting finding because it demonstrated that the catalytic function of phosphatase can be mimicked by simply replicating the helical structure of the natural catalytic domain. The finding also gives rise to the possibility that the earliest enzymes might have been formed from short peptides or polymers with repeating amino acid sequences that relied on self-assembly to achieve a folded structure because the environment at the beginning of protein evolution is too harsh for the biosynthesis of macromolecules with delicate structure and cofactors.<sup>58,59</sup> Eventually, with respect to bioinspiration, the catalytic behaviors of the helical short peptide assemblies confirmed the feasibility of phosphatase-like supramolecular catalysis.

**2.4. Structure–Activity Relationship.** The different catalytic performances of helical and  $\beta$ -sheet assemblies toward phosphoester substrates reflected the different structure–function relationships. In natural proteins, all of the hydrogen bonds in  $\alpha$ -helix motifs point to the same direction because the peptide units align in the same orientation along the helical axis. Peptide units have dipole moments that arise from the different polarities of N–H and C=O groups, and these

dipole moments are also aligned along the helical axis. The overall effect is a significant net dipole for the  $\alpha$ -helix, which produces a partial positive charge at the amino end and a partial negative charge at the carboxy end.<sup>60</sup> For many phosphatases, phosphate moieties are frequently found to bind to the N-terminal of an  $\alpha$ -helix (as illustrated in Scheme 1a), which corresponds to the optimal interaction between the helix dipole and the phosphate group.<sup>28,61–63</sup> Herein, the density functional theory (DFT) calculation was carried out to analyze the dipoles of the designed heptapeptide helices. As shown in Figure 4a, although Hept-SH and Hept-HS folds are not typical  $\alpha$ -helix in configuration, dipoles were also found along the helical axis in both helices. Molecular electrostatic potential (MEP) analysis revealed that the N-terminal of the helices is obviously positively charged (Figure S17), which causes a strong electrostatic attraction toward the negatively charged phosphate group. This interaction not only benefits the orientation of the substrate but also helps to reduce the potential energy of the phosphate group, making it prone to attack from the nucleophile serine. The role of helical dipole moment for phosphatase-like catalysis is also demonstrated by the helical assemblies built from the N-terminal-acetyl or C-terminal-amidated Hept-SH derivatives (Figure S18). In the  $\beta$ -sheet structure, the dipole moments derived from intermo-

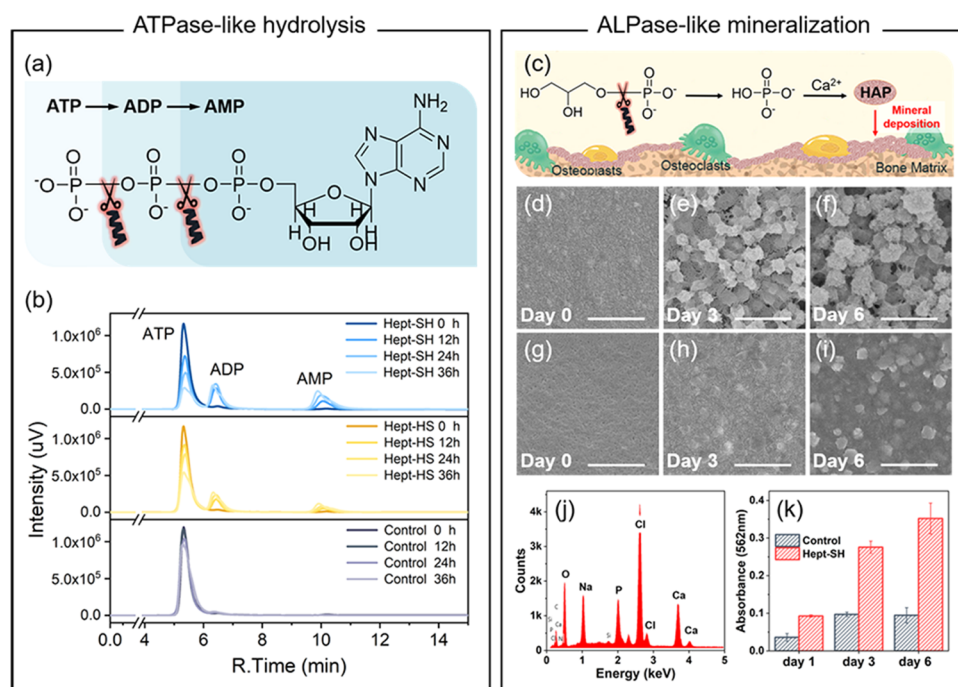


**Figure 5.** (a) Two-step hydrolysis from ATP through ADP to AMP catalyzed by helical assemblies. (b) HPLC chromatography of the hydrolysis of ATP. (c) Biomimetic hydroxyapatite mineralization reaction catalyzed by helical assemblies. (d–f) SEM images of mineral deposits on the surface covered with Hept-SH assembly and (g–i) the blank surface. The scale bar is 1  $\mu\text{m}$ . (j) EDX analysis of the mineralized nodules. (k) Quantification of the deposited calcium on glass surfaces by the Alizarin Red S method.

lecular hydrogen bonds almost offset each other (Figure S19).<sup>64</sup> Unless specially designed, it is unusual for the  $\beta$ -sheet structure to attract or reduce the potential energy of phosphate substrates. We speculated that the electrostatic pattern of the helix is highly conducive to Hept-SH species, in which the serine is located exactly at the N-terminal of the helix, making it more convenient to conduct a nucleophilic attack through its deprotonated hydroxyl. However, for Hept-HS species, the serine residue is located in the middle of the helix, which is a less favorable configuration. This might explain the higher catalytic efficiency of Hept-SH than that of Hept-HS.

The formation of supramolecular assemblies often contributes to the enzymatic enhancement for many catalytic assemblies.<sup>65–67</sup> In this study, we observed that the formation of Hept-SH and Hept-HS assemblies is a time-dependent process (Figures S20 and S21). Meanwhile, we detected the catalytic activity during the assembly. Figure 4b shows that free peptides are inactive on the first day (0 day), while the catalytic ability ( $V_{0-pNPP}$ ) starts to increase once primitive aggregates are formed (1–2 day), and the activities reach the maximum when the self-assembly is completed (after 5 days). A filtration experiment was performed to separate the mature assemblies from free monomers and oligomers, which also verified that the assemblies contribute to the catalytic ability, rather than the monomers or oligomers in the filtrate (Figure S22). Besides, Figure S23 demonstrates that the free catalytic groups (e.g., free imidazole, free His, Ser, Aib, or the combinations of the amino acids) are inactive for the hydrolytic reaction, which verified that the simple mixture of active residues is invalid for catalysis. In addition, the sedimentation experiment further demonstrates that the well-ordered self-assembly is essential for the active species because the amorphous peptide floccules are inactive whether they are incubated or not (Figure S24). These results reflect that the phosphatase-like activity is closely

associated with the formation of well-ordered supramolecular assemblies.

Single-crystal X-ray diffraction analysis demonstrated the hierarchical organization of heptapeptide helices within the assemblies. For both heptapeptides, the twin helical monomers interacted with each other to form coiled-coil dimers in a parallel orientation, driven by the hydrophobic and aromatic interactions of the phenylalanine zipper within the  $a$ – $d$  face. It is observed that the Hept-SH helices interlace tighter in the dimer than Hept-HS because of the stretchable phenylalanine side chains within the  $a$ – $d$  face. In contrast, the phenylalanine side chains in Hept-HS blocked the close packing of twin helices due to the restriction of intramolecular hydrogen bonds (Figure S25).

Due to the different arrangement of the helical dimer, the dimeric units adopt a different packing pattern when they propagate to form a continuous array of supramolecular assemblies. For Hept-SH, the dimeric unit repeats itself along the  $a$ -axis and  $b$ -axis (Figure S26, note: the angle between the  $a$ -axis and  $b$ -axis is  $120^\circ$ ). While in the  $c$ -direction, the Hept-SH dimer rotates twice around the  $c$ -axis, forming a 3-dimer stack with an angle of  $120^\circ$  (Figure 4c). As a result, the dimers formed a cylinder along the  $c$ -axis, and these cylinders further organized into high-ordered assemblies. Unlike Hept-SH dimers, the twin Hept-HS helices formed “/ \”-type dimers, which leads to the alternate packing of antiparallel dimers along the  $c$ -axis (Figure 4d). This arrangement was repeated and well-aligned in direction  $a$  but staggered from the view of the  $b$ -direction (Figure S27), which exhibited a completely different packing mode from Hept-SH assemblies. For both assemblies, the well-ordered aggregations of dimers are stabilized either through the hydrogen bonds between the head-to-tail backbone or the hydrogen bonds within the hydrophilic faces. Additionally, upon self-assembly, the

histidine residue, serine residue, and carboxyl at the C-terminal from different dimers approach each other spatially, which is favorable to form a triad for substrate binding and catalysis (Figure 4e,f).

Based on the crystal structure of supramolecular assemblies, molecule docking was carried out to get an insight into the binding of *p*NPP in the catalytic domain (Figure S28). For Hept-SH assemblies, the phosphate group embedded into the gap between helical dimers, binding to His4 and the C-terminal carboxyl (Aib7) through intermolecular hydrogen bonds within 4 Å, which implied the possible catalytic mechanism through the electrical transfer among the serine residue, histidine residue and carboxyl at the C-terminal. Remarkably, it was found that the substrate-bonded residues came from different helical dimers, which indicated the importance of supramolecular self-assembly in the formation of the catalytic center. Due to the combination of the helical structure and catalytic triad, the Hept-SH assemblies displayed favorable hydrolytic ability toward *p*NPP. For Hept-HS assemblies, *p*NPP suffered from steric hindrance within the array of antiparallel helical dimers. The distance between the phosphate group and the catalytic residues was farther (6–10 Å), leading to the inferior catalytic performance of Hept-HS assemblies compared with that of Hept-SH assemblies.

### 2.5. Catalytic Function as ATPase and ALPase Mimics.

Using *p*NPP as the model substrate, we have verified the competence of helical assemblies in the hydrolysis of the phosphoester bond in the absence of any metal cofactor. Based on the common existence of helical domains in the active center of phosphatase family, we further investigated the potential of this *de novo* designed catalytic module as specific phosphatase mimics in physiological reactions.

ATPase is a class of enzymes that catalyze the two-step hydrolysis of adenosine triphosphate (ATP) into adenosine diphosphate (ADP) and adenosine monophosphate (AMP). The breaking of phosphoester bonds produces energy that is required by many physiological processes (Figure 5a). The HPLC result indicated that Hept-SH and Hept-HS assemblies exhibited an obvious ATPase-like activity in the conversion of ATP → ADP → AMP (Figure 5b). Besides, Hept-SH assemblies exhibited superior catalytic activity compared with Hept-HS assemblies. A total of 69.13% of ATP was hydrolyzed by Hept-SH after 36 h, whereas only 44.05% hydrolyzation was achieved by Hept-HS. This result is consistent with the activity evaluation using *p*NPP as a substrate.

Bone formation is a complex process that requires ALPase at each level of this process. ALPase increases the inorganic phosphate/pyrophosphate ratio in the extracellular matrix through the nonspecific cleavage of phosphate esters. This reaction elevates the local concentration of inorganic phosphate and promotes the formation of hydroxyapatite (HAP, Ca<sub>5</sub>(PO<sub>4</sub>)<sub>3</sub>(OH)), which is an essential building block of bone and teeth (Figure 5c). Considering the phosphatase-like catalytic ability of Hept-SH assemblies, we envisage that they have great potential to simulate the osteogenic function of natural ALPase. To verify this, glass slides were coated with Hept-SH assemblies and then incubated in a solution containing β-glycerophosphate and CaCl<sub>2</sub>. SEM analysis (Figure 5d–f) revealed that during the incubation, nodal-like mineral deposits were gradually generated on the surface covered by Hept-SH. Energy-dispersive X-ray (EDX) spectral analysis indicated high calcium and phosphorus levels of mineralized nodules on the Hept-SH-coated surface, confirm-

ing the production of HAP (Figure 5j). As a control, only a small amount of irregular precipitates was formed on the blank glass surface (Figure 5g–i). The Alizarin Red S method was performed to quantify the amount of calcium deposited on glass surfaces. As shown in Figure 5k, the deposited calcium level on the Hept-SH-coated surface increased much faster than that on the blank surface, confirming the ALPase-like catalytic ability of Hept-SH species, which accelerated the hydrolysis of β-glycerophosphate.

## 3. CONCLUSIONS

After millions of years of evolution, existing enzymes are composed of at least hundreds of amino acid residues. Polypeptides with long sequences are thought to be able to form complicated structures upon molecular folding and thus possess recognition, accumulation, and catalytic functions. However, this consensus may be challenged by catalytic peptide assemblies. Many β-sheet-forming peptides, from tripeptides to 20-residue peptides, have been reported to be capable of catalyzing simple reactions under physiological conditions, through self-assembly with or without cofactors. These findings give rise to the possibility that short peptides with amyloid structures were the “primitive enzymes” on the early earth. In the case of helix-forming peptides, although helical peptides or coiled-coil bundles have also been used in the organization of enzyme-like catalysts, they merely act as the scaffolds for supporting catalytic residues or metal cofactors,<sup>68,69</sup> whereas the intrinsic features of the helical structure in enzymatic reactions are almost ignored. In this study, inspired by the helical structure in the metal-free phosphatase family, we have shown the *de novo* design and construction of a phosphatase mimic through the self-assembly of helical heptapeptides. In comparison with the β-sheet-organized species, we demonstrated the unique helical assemblies in the hydrolysis of the phosphoester bonds due to the helical-derived dipole moment and the supramolecular assembly. This study not only presented a strategy for the construction of phosphatase-like mimics but also extended the understanding of the role of helical structure in the evolution of primitive enzymes.

## 4. MATERIALS AND METHODS

**4.1. Materials.** Lyophilized heptapeptides (Hept-SH and Hept-HS) were purchased from the Top-Peptide Biotechnology (Shanghai) Co. Ltd. *p*-Nitrophenyl phosphate (*p*NPP), *p*-nitrophenyl acetate (*p*NPA), 5'-adenosine triphosphate disodium (ATP), β-glycerophosphate (BGP), and Alizarin Red S were purchased from the Aladdin Industrial Corp. (Shanghai, China). Other chemicals and solvents of analytical grade were obtained from commercial sources.

**4.2. Preparation of Heptapeptide Self-Assemblies.** Fresh peptide stock solutions were prepared by dissolving 3 μmol of heptapeptide in 20 μL of DMSO and diluting the solution with 980 μL of Tris–HCl buffer (10 mM, pH7.4) to a final peptide concentration of 3 mM. Then, the solutions were thoroughly mixed and incubated at room temperature.

**4.3. Catalytic Reaction and Kinetic Assays.** In a typical experiment of *p*NPP hydrolysis, 3 mM incubated peptide stock solution was diluted with Tris–HCl buffer (25 mM, pH7.4), and freshly prepared *p*NPP stock solution (dissolved in ddH<sub>2</sub>O) under different concentrations was added before the measurement of absorbance at 400 nm. The final concen-

tration of the peptide is 0.08 mM, and the concentration of pNPP is 0.1–8 mM. Two hundred microliters of the reactant was added in a 96-well microplate well for a time-dependent absorbance reading under 37 °C. The data was background corrected (self-hydrolyzation without peptide catalysts), and errors were obtained from the standard deviation of three repeats. The hydrolysis of pNPA was carried out under the same peptide/substrate concentration, and the pNPA stock solution was dissolved in acetonitrile.

Enzymatic kinetic assays were studied by fitting the Michaelis–Menten equation to give a three-state curve as well as kinetic parameters.<sup>70</sup> To obtain accurate  $K_m$  and  $k_{cat}$  values, Lineweaver–Burk plots were performed to calculate kinetic parameters (peptide assemblies 0.08 mM, substrate 0.9–8 mM).<sup>71</sup>

**4.4. Transmission Electron Microscopy (TEM).** Morphologies of peptide self-assemblies were collected using a JEM-2100F (JEOL Ltd., Japan) electron microscope under 200 kV. Five microliters of an aliquot of the stock solution of peptide assembly was used for the sample preparation on 200 meshes carbon-coated copper grid, and the sample was negatively stained with 2% uranyl acetate.

**4.5. Circular Dichroism (CD).** In CD experiments, DMSO used in the peptide assembly preparation was substituted by HFIP to eliminate the background signal. The assembled peptides were diluted to 0.75 mM and tested in a 0.1 mm path length quartz cuvette. Circular dichroism spectra in the range of 190–260 nm were recorded on a J-810 CD spectropolarimeter (JASCO, Japan). The background-subtracted data was converted from ellipticity (deg) to molar ellipticity (MER; deg cm<sup>2</sup> dmol<sup>-1</sup> res<sup>-1</sup>) by normalizing for the peptide bond concentration and the cell path length. The temperature stability of the peptide secondary structure was tested between 20 and 90 °C with a heating–cooling program. After reaching the desired temperature, the samples were incubated for 10 min before spectral scanning.

**4.6. Crystal Structure Analysis.** Colorless diffraction quality crystals were grown by slowly evaporating solvent from solutions containing 3 mM peptide at room temperature. Single-crystal X-ray diffraction data were collected on a Bruker SMART APEX II diffractometer with Cu K $\alpha$ 1 ( $\lambda = 1.5418$  Å) radiation. The structure was refined by full-matrix least-squares against F<sup>2</sup> with SHELXL-2013. The crystallographic data are summarized in Table S4. The CIF for each structure is uploaded in the Supporting Information.

**4.7. ATP Hydrolysis.** Assembled heptapeptide stocks were dispersed in Tris–HCl buffer (10 mM, pH 7.4) to a final concentration of 0.5 mM, and the reaction concentration of the substrate 5'-adenosine triphosphate disodium (ATP) was 1 mM. The reaction was kept at 25 °C. During the reaction, the composition of the reactant was measured using high-performance liquid chromatography (LC-20A, Shimadzu, Japan) equipped with a reverse-phase C18 column. The eluent was a potassium phosphate buffer (50 mM, pH 6.5) with a flow rate of 0.8 mL min<sup>-1</sup>, and the detection wavelength was 254 nm using a UV detector.

**4.8. Biomineralization.** Clean glass slides were coated with 0.5 mM Hept-SH peptide stock solution, and the mineralization was conducted in 24-well plates. In each well, 800  $\mu$ L of osteogenic solution containing 15 mM of  $\beta$ -glycerophosphate (Pi source) and 20 mM of CaCl<sub>2</sub> (Ca<sup>2+</sup> source) in Tris–HCl buffer (25 mM, pH 7.4) was added. Incubation was conducted at room temperature. Once a day,

the osteogenic solution was removed from the surface and replaced with a fresh one. After 6 days, the supernatant was removed, and the slides were rinsed with ddH<sub>2</sub>O 3 times and air-dried. The slides were stained with 0.1% Alizarin Red S for 20 min to quantify the mineralized calcium. After that, the slides were washed with ddH<sub>2</sub>O 3 times, and the calcium-bound dye was then extracted by 10% cetylpyridinium chloride for 20 min. Finally, the mineralized calcium can be estimated by directly determining the absorbance of Alizarin Red S at 562 nm using a UV–vis spectrophotometer (TU-1900, Persee Devices, China).

The mineralized slides are directly dried in air and sputter-coated with platinum before scanning electron microscopy (SEM) characterization. Images were recorded on an S-4800 field emission SEM (Hitachi High-Technologies Co., Japan) at an acceleration voltage of 3 kV, and the element analysis was conducted on the EDX module.

## ■ ASSOCIATED CONTENT

### SI Supporting Information

The Supporting Information is available free of charge at <https://pubs.acs.org/doi/10.1021/acscatal.1c00129>.

Additional methods of secondary structure characterization, computational calculation, AFM, pyrene fluorescence, and sedimentation experiment; Supporting data, figures, and tables about molecular characterization (HPLC and ESI-MS), secondary structure (FTIR, Raman, NMR, and CD), kinetic studies, active studies, calculation results, and crystal information (PDF)

## ■ AUTHOR INFORMATION

### Corresponding Authors

**Mengfan Wang** – School of Chemical Engineering and Technology, State Key Laboratory of Chemical Engineering, Tianjin University, Tianjin 300350, P. R. China; Tianjin Key Laboratory of Membrane Science and Desalination Technology, Tianjin 300350, P. R. China; Email: [mwang@tju.edu.cn](mailto:mwang@tju.edu.cn)

**Wei Qi** – School of Chemical Engineering and Technology, State Key Laboratory of Chemical Engineering, Tianjin University, Tianjin 300350, P. R. China; The Co-Innovation Centre of Chemistry and Chemical Engineering of Tianjin, Tianjin 300072, P. R. China; Tianjin Key Laboratory of Membrane Science and Desalination Technology, Tianjin 300350, P. R. China; [orcid.org/0000-0002-7378-1392](https://orcid.org/0000-0002-7378-1392); Email: [qiwei@tju.edu.cn](mailto:qiwei@tju.edu.cn)

### Authors

**Yutong Wang** – School of Chemical Engineering and Technology, State Key Laboratory of Chemical Engineering, Tianjin University, Tianjin 300350, P. R. China

**Lijun Yang** – School of Chemical Engineering and Technology, State Key Laboratory of Chemical Engineering, Tianjin University, Tianjin 300350, P. R. China

**Jiaying Zhang** – School of Chemical Engineering and Technology, State Key Laboratory of Chemical Engineering, Tianjin University, Tianjin 300350, P. R. China

**Rongxin Su** – School of Chemical Engineering and Technology, State Key Laboratory of Chemical Engineering, Tianjin University, Tianjin 300350, P. R. China; The Co-Innovation Centre of Chemistry and Chemical Engineering of Tianjin, Tianjin 300072, P. R. China; Tianjin Key

Laboratory of Membrane Science and Desalination Technology, Tianjin 300350, P. R. China; [orcid.org/0000-0001-9778-9113](https://orcid.org/0000-0001-9778-9113)

Zhimin He – School of Chemical Engineering and Technology, State Key Laboratory of Chemical Engineering, Tianjin University, Tianjin 300350, P. R. China

Complete contact information is available at:  
<https://pubs.acs.org/10.1021/acscatal.1c00129>

## Notes

The authors declare no competing financial interest.

## ACKNOWLEDGMENTS

This work was financially supported by the National Natural Science Foundation of China (21621004 and 21676191). The authors gratefully acknowledge Dr. Lin Zhi from the School of Life Sciences, Tianjin University, for his valuable advices on the NMR analysis.

## REFERENCES

- (1) Lewis, C. A.; Gustafson, J. L.; Chiu, A.; Balsells, J.; Pollard, D.; Murry, J.; Reamer, R. A.; Hansen, K. B.; Miller, S. J. A Case of Remote Asymmetric Induction in the Peptide-Catalyzed Desymmetrization of a Bis(phenol). *J. Am. Chem. Soc.* **2008**, *130*, 16358–16365.
- (2) Metrano, A. J.; Chinn, A. J.; Shugrue, C. R.; Stone, E. A.; Kim, B.; Miller, S. J. Asymmetric Catalysis Mediated by Synthetic Peptides, Version 2.0: Expansion of Scope and Mechanisms. *Chem. Rev.* **2020**, *120*, 11479–11615.
- (3) Zozulia, O.; Dolan, M. A.; Korendovych, I. V. Catalytic peptide assemblies. *Chem. Soc. Rev.* **2018**, *47*, 3621–3639.
- (4) Biniuri, Y.; Albada, B.; Wolff, M.; Golub, E.; Gelman, D.; Willner, I. Cu<sup>2+</sup> or Fe<sup>3+</sup> Terpyridine/Aptamer Conjugates: Nucleoapzymes Catalyzing the Oxidation of Dopamine to Aminochrome. *ACS Catal.* **2018**, *8*, 1802–1809.
- (5) Liu, J.; Cao, Z.; Lu, Y. Functional Nucleic Acid Sensors. *Chem. Rev.* **2009**, *109*, 1948–1998.
- (6) Silverman, S. K. Catalytic DNA: Scope, Applications, and Biochemistry of Deoxyribozymes. *Trends Biochem. Sci.* **2016**, *41*, 595–609.
- (7) Xu, B.; Wang, H.; Wang, W.; Gao, L.; Li, S.; Pan, X.; Wang, H.; Yang, H.; Meng, X.; Wu, Q.; Zheng, L.; Chen, S.; Shi, X.; Fan, K.; Yan, X.; Liu, H. A Single-Atom Nanozyme for Wound Disinfection Applications. *Angew. Chem., Int. Ed.* **2019**, *58*, 4911–4916.
- (8) Luo, L.; Huang, L.; Liu, X.; Zhang, W.; Yao, X.; Dou, L.; Zhang, X.; Nian, Y.; Sun, J.; Wang, J. Mixed-Valence Ce-BPyDC Metal–Organic Framework with Dual Enzyme-like Activities for Colorimetric Biosensing. *Inorg. Chem.* **2019**, *58*, 11382–11388.
- (9) Wang, D.; Wu, H.; Lim, W. Q.; Phua, S. Z. F.; Xu, P.; Chen, Q.; Guo, Z.; Zhao, Y. A Mesoporous Nanoenzyme Derived from Metal–Organic Frameworks with Endogenous Oxygen Generation to Alleviate Tumor Hypoxia for Significantly Enhanced Photodynamic Therapy. *Adv. Mater.* **2019**, *31*, No. 1901893.
- (10) Gao, L.; Zhuang, J.; Nie, L.; Zhang, J.; Zhang, Y.; Gu, N.; Wang, T.; Feng, J.; Yang, D.; Perrett, S.; Yan, X. Intrinsic peroxidase-like activity of ferromagnetic nanoparticles. *Nat. Nanotechnol.* **2007**, *2*, 577–583.
- (11) Natalio, F.; André, R.; Hartog, A. F.; Stoll, B.; Jochum, K. P.; Wever, R.; Tremel, W. Vanadium pentoxide nanoparticles mimic vanadium haloperoxidases and thwart biofilm formation. *Nat. Nanotechnol.* **2012**, *7*, 530–535.
- (12) Singh, N.; Savanur, M. A.; Srivastava, S.; D’Silva, P.; Mughesh, G. A Redox Modulatory Mn<sub>3</sub>O<sub>4</sub> Nanozyme with Multi-Enzyme Activity Provides Efficient Cytoprotection to Human Cells in a Parkinson’s Disease Model. *Angew. Chem., Int. Ed.* **2017**, *56*, 14267–14271.
- (13) Yao, X.; Liu, T.; Xie, Y.; Chu, Z.; Jin, W. In Situ-Forming Magnetic Fe<sub>3</sub>O<sub>4</sub> Nanoroses on Defect-Controllable Mesoporous Graphene Oxide for Enzyme-Mimic Sensing. *Ind. Eng. Chem. Res.* **2020**, *59*, 17934–17943.
- (14) He, Q.; Kelliher, M.; Bähring, S.; Lynch, V. M.; Sessler, J. L. A Bis-calix[4]pyrrole Enzyme Mimic That Constrains Two Oxoanions in Close Proximity. *J. Am. Chem. Soc.* **2017**, *139*, 7140–7143.
- (15) Burton, A. J.; Thomson, A. R.; Dawson, W. M.; Brady, R. L.; Woolfson, D. N. Installing hydrolytic activity into a completely de novo protein framework. *Nat. Chem.* **2016**, *8*, 837–844.
- (16) Liu, Q.; Wan, K.; Shang, Y.; Wang, Z.-G.; Zhang, Y.; Dai, L.; Wang, C.; Wang, H.; Shi, X.; Liu, D.; Ding, B. Cofactor-free oxidase-mimetic nanomaterials from self-assembled histidine-rich peptides. *Nat. Mater.* **2021**, *20*, 395–402.
- (17) Nothling, M. D.; Xiao, Z.; Bhaskaran, A.; Blyth, M. T.; Bennett, C. W.; Coote, M. L.; Connal, L. A. Synthetic Catalysts Inspired by Hydrolytic Enzymes. *ACS Catal.* **2019**, *9*, 168–187.
- (18) Metrano, A. J.; Abascal, N. C.; Mercado, B. Q.; Paulson, E. K.; Hurtley, A. E.; Miller, S. J. Diversity of Secondary Structure in Catalytic Peptides with  $\beta$ -Turn-Biased Sequences. *J. Am. Chem. Soc.* **2017**, *139*, 492–516.
- (19) Colombo, G.; Soto, P.; Gazit, E. Peptide self-assembly at the nanoscale: a challenging target for computational and experimental biotechnology. *Trends Biotechnol.* **2007**, *25*, 211–218.
- (20) Wang, J.; Liu, K.; Xing, R.; Yan, X. Peptide self-assembly: thermodynamics and kinetics. *Chem. Soc. Rev.* **2016**, *45*, 5589–5604.
- (21) Rhys, G. G.; Wood, C. W.; Beesley, J. L.; Zaccari, N. R.; Burton, A. J.; Brady, R. L.; Thomson, A. R.; Woolfson, D. N. Navigating the Structural Landscape of De Novo  $\alpha$ -Helical Bundles. *J. Am. Chem. Soc.* **2019**, *141*, 8787–8797.
- (22) Rufo, C. M.; Moroz, Y. S.; Moroz, O. V.; Stöhr, J.; Smith, T. A.; Hu, X.; DeGrado, W. F.; Korendovych, I. V. Short peptides self-assemble to produce catalytic amyloids. *Nat. Chem.* **2014**, *6*, 303.
- (23) Wong, Y.-M.; Masunaga, H.; Chuah, J.-A.; Sudesh, K.; Numata, K. Enzyme-Mimic Peptide Assembly To Achieve Amidolytic Activity. *Biomacromolecules* **2016**, *17*, 3375–3385.
- (24) Mou, Y.; Yu, J.-Y.; Wannier, T. M.; Guo, C.-L.; Mayo, S. L. Computational design of co-assembling protein–DNA nanowires. *Nature* **2015**, *525*, 230–233.
- (25) Li, F.; Li, Y.; Zhou, Z.; Lv, S.; Deng, Q.; Xu, X.; Yin, L. Engineering the aromaticity of cationic helical polypeptides toward “self-activated” DNA/siRNA delivery. *ACS Appl. Mater. Interfaces* **2017**, *9*, 23586–23601.
- (26) Wolfenden, R. Benchmark reaction rates, the stability of biological molecules in water, and the evolution of catalytic power in enzymes. *Annu. Rev. Biochem.* **2011**, *80*, 645–667.
- (27) Yu, Z.-H.; Zhang, Z.-Y. Regulatory Mechanisms and Novel Therapeutic Targeting Strategies for Protein Tyrosine Phosphatases. *Chem. Rev.* **2018**, *118*, 1069–1091.
- (28) Hirsch, A. K.; Fischer, F. R.; Diederich, F. Phosphate recognition in structural biology. *Angew. Chem., Int. Ed.* **2007**, *46*, 338–352.
- (29) Dillet, V.; Van Etten, R. L.; Bashford, D. Stabilization of Charges and Protonation States in the Active Site of the Protein Tyrosine Phosphatases: A Computational Study. *J. Phys. Chem. B* **2000**, *104*, 11321–11333.
- (30) Ljubetič, A.; Lapenta, F.; Gradišar, H.; Drobnak, I.; Aupič, J.; Strmšek, Z.; Lainšček, D.; Hafner-Bratkovič, I.; Majerle, A.; Krivec, N.; Benčina, M.; Pisanski, T.; Veličković, T. Č.; Round, A.; Carazo, J. M.; Melero, R.; Jerala, R. Design of coiled-coil protein-origami cages that self-assemble in vitro and in vivo. *Nat. Biotechnol.* **2017**, *35*, 1094–1101.
- (31) Lupas, A. Coiled coils: new structures and new functions. *Trends Biochem. Sci.* **1996**, *21*, 375–382.
- (32) Woolfson, D. N. In *Fibrous Proteins: Structures and Mechanisms*; Parry, D. A. D.; Squire, J. M., Eds.; Springer International Publishing: Cham, 2017; pp 35–61.
- (33) Mondal, S.; Adler-Abramovich, L.; Lampel, A.; Bram, Y.; Lipstman, S.; Gazit, E. Formation of functional super-helical

assemblies by constrained single heptad repeat. *Nat. Commun.* **2015**, *6*, No. 8615.

(34) Jones, J. E.; Diemer, V.; Adam, C.; Rafferty, J.; Ruscoe, R. E.; Sengel, J. T.; Wallace, M. I.; Bader, A.; Cockroft, S. L.; Clayden, J.; Webb, S. J. Length-Dependent Formation of Transmembrane Pores by  $3_{10}$ -Helical  $\alpha$ -Aminoisobutyric Acid Foldamers. *J. Am. Chem. Soc.* **2016**, *138*, 688–695.

(35) Buller, A. R.; Townsend, C. A. Intrinsic evolutionary constraints on protease structure, enzyme acylation, and the identity of the catalytic triad. *Proc. Natl. Acad. Sci. U.S.A.* **2013**, *110*, E653.

(36) Miles, A. J.; Wallace, B. A. Circular dichroism spectroscopy of membrane proteins. *Chem. Soc. Rev.* **2016**, *45*, 4859–4872.

(37) Mondal, S.; Adler-Abramovich, L.; Lampel, A.; Bram, Y.; Lipstman, S.; Gazit, E. Formation of functional super-helical assemblies by constrained single heptad repeat. *Nat. Commun.* **2015**, *6*, No. 8615.

(38) Goodman, M.; Toniolo, C.; Peggion, E. Conformational aspects of polypeptides. XXIX. Conformational assignments for some aromatic polypeptides by far-uv cotton effects. New results. *Biopolymers* **1968**, *6*, 1691–1695.

(39) Chin, D.-H.; Woody, R. W.; Rohl, C. A.; Baldwin, R. L. Circular dichroism spectra of short, fixed-nucleus alanine helices. *Proc. Natl. Acad. Sci. U.S.A.* **2002**, *99*, 15416.

(40) Shepherd, N. E.; Hoang, H. N.; Abbenante, G.; Fairlie, D. P. Single Turn Peptide Alpha Helices with Exceptional Stability in Water. *J. Am. Chem. Soc.* **2005**, *127*, 2974–2983.

(41) Chen, Y.; Viereck, J.; Harmer, R.; Rangan, S.; Bartynski, R. A.; Galoppini, E. Helical Peptides Design for Molecular Dipoles Functionalization of Wide Band Gap Oxides. *J. Am. Chem. Soc.* **2020**, *142*, 3489–3498.

(42) Ji, W.; Yuan, C.; Chakraborty, P.; Gilead, S.; Yan, X.; Gazit, E. Stoichiometry-controlled secondary structure transition of amyloid-derived supramolecular dipeptide co-assemblies. *Commun. Chem.* **2019**, *2*, No. 65.

(43) Dolui, S.; Mondal, A.; Roy, A.; Pal, U.; Das, S.; Saha, A.; Maiti, N. C. Order, Disorder, and Reorder State of Lysozyme: Aggregation Mechanism by Raman Spectroscopy. *J. Phys. Chem. B* **2020**, *124*, 50–60.

(44) Polizzi, N. F.; Wu, Y.; Lemmin, T.; Maxwell, A. M.; Zhang, S.-Q.; Rawson, J.; Beratan, D. N.; Therien, M. J.; DeGrado, W. F. De novo design of a hyperstable non-natural protein–ligand complex with sub-Å accuracy. *Nat. Chem.* **2017**, *9*, 1157–1164.

(45) Ulas, G.; Lemmin, T.; Wu, Y.; Gassner, G. T.; DeGrado, W. F. Designed metalloprotein stabilizes a semiquinone radical. *Nat. Chem.* **2016**, *8*, 354–359.

(46) Gratias, R.; Konat, R.; Kessler, H.; Crisma, M.; Valle, G.; Polese, A.; Formaggio, F.; Toniolo, C.; Broxterman, Q. B.; Kamphuis, J. First Step Toward the Quantitative Identification of Peptide  $3_{10}$ -Helix Conformation with NMR Spectroscopy: NMR and X-ray Diffraction Structural Analysis of a Fully-Developed  $3_{10}$ -Helical Peptide Standard. *J. Am. Chem. Soc.* **1998**, *120*, 4763–4770.

(47) Mensch, C.; Barron, L. D.; Johannessen, C. Ramachandran mapping of peptide conformation using a large database of computed Raman and Raman optical activity spectra. *Phys. Chem. Chem. Phys.* **2016**, *18*, 31757–31768.

(48) Ganguly, A.; Luong, T. Q.; Brylski, O.; Dirkmann, M.; Möller, D.; Ebbinghaus, S.; Schulz, F.; Winter, R.; Sanchez-Garcia, E.; Thiel, W. Elucidation of the Catalytic Mechanism of a Miniature Zinc Finger Hydrolase. *J. Phys. Chem. B* **2017**, *121*, 6390–6398.

(49) Cleland, W. W.; Hengge, A. C. Enzymatic mechanisms of phosphate and sulfate transfer. *Chem. Rev.* **2006**, *106*, 3252–3278.

(50) Roskoski, R. Michaelis-Menten Kinetics. In *Reference Module in Biomedical Sciences* 2015.

(51) Wang, M.; Lv, Y.; Liu, X.; Qi, W.; Su, R.; He, Z. Enhancing the activity of peptide-based artificial hydrolase with catalytic Ser/His/Asp triad and molecular imprinting. *ACS Appl. Mater. Interfaces* **2016**, *8*, 14133–14141.

(52) Zhao, Y.; Lei, B.; Wang, M.; Wu, S.; Qi, W.; Su, R.; He, Z. A supramolecular approach to construct a hydrolase mimic with photo-switchable catalytic activity. *J. Mater. Chem. B* **2018**, *6*, 2444–2449.

(53) Makam, P.; Yamijala, S. S.; Tao, K.; Shimon, L. J.; Eisenberg, D. S.; Sawaya, M. R.; Wong, B. M.; Gazit, E. Non-proteinaceous hydrolase comprised of a phenylalanine metallo-supramolecular amyloid-like structure. *Nat. Catal.* **2019**, *2*, 977–985.

(54) Gulseren, G.; Yasa, I. C.; Ustahuseyin, O.; Tekin, E. D.; Tekinay, A. B.; Guler, M. O. Alkaline phosphatase-mimicking peptide nanofibers for osteogenic differentiation. *Biomacromolecules* **2015**, *16*, 2198–2208.

(55) Olguin, L. F.; Askew, S. E.; O'Donoghue, A. C.; Hollfelder, F. Efficient Catalytic Promiscuity in an Enzyme Superfamily: An Arylsulfatase Shows a Rate Acceleration of 1013 for Phosphate Monoester Hydrolysis. *J. Am. Chem. Soc.* **2008**, *130*, 16547–16555.

(56) Menzinger, M.; Wolfgang, R. The meaning and use of the Arrhenius activation energy. *Angew. Chem., Int. Ed.* **1969**, *8*, 438–444.

(57) Madan, L. L.; Gopal, B. Conformational Basis for Substrate Recruitment in Protein Tyrosine Phosphatase 10D. *Biochemistry* **2011**, *50*, 10114–10125.

(58) Romero Romero, M. L.; Rabin, A.; Tawfik, D. S. Functional Proteins from Short Peptides: Dayhoff's Hypothesis Turns 50. *Angew. Chem., Int. Ed.* **2016**, *55*, 15966–15971.

(59) Greenwald, J.; Kwiatkowski, W.; Riek, R. Peptide Amyloids in the Origin of Life. *J. Mol. Biol.* **2018**, *430*, 3735–3750.

(60) Ganesan, S. J.; Matysiak, S. Role of Backbone Dipole Interactions in the Formation of Secondary and Supersecondary Structures of Proteins. *J. Chem. Theory. Comput.* **2014**, *10*, 2569–2576.

(61) Longo, L. M.; Petrović, D.; Kamerlin, S. C. L.; Tawfik, D. S. Short and simple sequences favored the emergence of N-helix phospho-ligand binding sites in the first enzymes. *Proc. Natl. Acad. Sci. U.S.A.* **2020**, *117*, 5310.

(62) Petrović, D.; Risso, V. A.; Kamerlin, S. C. L.; Sanchez-Ruiz, J. M. Conformational dynamics and enzyme evolution. *J. R. Soc., Interface* **2018**, *15*, No. 20180330.

(63) Querol-García, J.; Fernández, F. J.; Marin, A. V.; Gómez, S.; Fullà, D.; Melchor-Tafur, C.; Franco-Hidalgo, V.; Albertí, S.; Juanhuix, J.; Rodríguez de Córdoba, S.; Regueiro, J. R.; Vega, M. C. Crystal Structure of Glyceraldehyde-3-Phosphate Dehydrogenase from the Gram-Positive Bacterial Pathogen *A. vaginae*, an Immunoevasive Factor that Interacts with the Human C5a Anaphylatoxin. *Front. Microbiol.* **2017**, *8*, 541.

(64) Hol, W. G.; Halie, L. M.; Sander, C. Dipoles of the  $\alpha$ -helix and  $\beta$ -sheet: their role in protein folding. *Nature* **1981**, *294*, 532–536.

(65) Song, R.; Wu, X.; Xue, B.; Yang, Y.; Huang, W.; Zeng, G.; Wang, J.; Li, W.; Cao, Y.; Wang, W.; et al. Principles governing catalytic activity of self-assembled short peptides. *J. Am. Chem. Soc.* **2019**, *141*, 223–231.

(66) Zhang, C.; Shafi, R.; Lampel, A.; MacPherson, D.; Pappas, C. G.; Narang, V.; Wang, T.; Maldarelli, C.; Ulijn, R. V. Switchable hydrolase based on reversible formation of supramolecular catalytic site using a self-assembling peptide. *Angew. Chem., Int. Ed.* **2017**, *56*, 14511–14515.

(67) Zhang, C.; Xue, X.; Luo, Q.; Li, Y.; Yang, K.; Zhuang, X.; Jiang, Y.; Zhang, J.; Liu, J.; Zou, G.; Liang, X.-J. Self-Assembled Peptide Nanofibers Designed as Biological Enzymes for Catalyzing Ester Hydrolysis. *ACS Nano* **2014**, *8*, 11715–11723.

(68) Rink, W. M.; Thomas, F. De Novo Designed  $\alpha$ -Helical Coiled-Coil Peptides as Scaffolds for Chemical Reactions. *Chem. – Eur. J.* **2019**, *25*, 1665–1677.

(69) Lombardi, A.; Pirro, F.; Maglio, O.; Chino, M.; DeGrado, W. F. De Novo Design of Four-Helix Bundle Metalloproteins: One Scaffold, Diverse Reactivities. *Acc. Chem. Res.* **2019**, *52*, 1148–1159.

(70) Bisswanger, H. From Reaction Order to the Michaelis–Menten Law: Fundamental Relationships of Enzyme Kinetics. In *Enzyme Kinetics*; John Wiley & Sons, Inc., 2017; pp 55–86.

(71) Lineweaver, H.; Burk, D. The determination of enzyme dissociation constants. *J. Am. Chem. Soc.* **1934**, *56*, 658–666.